Novel electrochemical process for the deposition of nanocrystalline $NiFe_2O_4$ thin films

2004 J. Phys.: Condens. Matter 16 773

(http://iopscience.iop.org/0953-8984/16/6/008)

INSTITUTE OF PHYSICS PUBLISHING JOURNAL OF PHYSICS: CONDENSED MATTER

J. Phys.: Condens. Matter **16** (2004) 773–784 PII: S0953-8984(04)68480-3

Novel electrochemical process for the deposition of nanocrystalline $NiFe_2O_4$ thin films

S D Sartale[1,4], C D Lokhande[2,5], M Giersig[1] and V Ganesan[3]

[1] Hahn Meitner Institute, Glienicker Strasse 100, D-14109, Berlin, Germany
[2] Thin Film Physics Laboratory, Department of Physics, Shivaji University, Kolhapur-416004 (MS), India
[3] Low Temperature Laboratory, Inter University Consortium, DAE Facilities, Indore-452 017 (MP), India

E-mail: sdsartale@yahoo.com

Received 4 September 2003, in final form 10 December 2003
Published 30 January 2004
Online at stacks.iop.org/JPhysCM/16/773 (DOI: 10.1088/0953-8984/16/6/008)

Abstract

Electrodeposition of $NiFe_2$ alloy from a non-aqueous ethylene glycol sulfate bath followed by electrochemical oxidation (anodization) of the alloy in an aqueous bath at room temperature is described as a novel electrochemical process to deposit spinel nanocrystalline $NiFe_2O_4$ thin films on different conducting substrates. Various electrochemical parameters such as bath composition, current density, deposition time and bath temperature for electrodeposition of the $NiFe_2$ alloy and its anodization have been studied and optimized to obtain good quality $NiFe_2O_4$ films. The crystal structure, composition, surface morphology and microstructure of the films have been studied using a variety of techniques. Air annealing of the as-deposited $NiFe_2O_4$ thin films at 500 °C for 5 h improves the crystallinity and morphology of the films.

1. Introduction

$NiFe_2O_4$ is the most suitable material for device applications in the upper microwave and lower millimetre wave ranges [1, 2]. Apart from its technological importance in the electronic and magnetic industries, $NiFe_2O_4$ has been used as a highly reproducible humidity [3] and gas [4, 5] sensor material.

$NiFe_2O_4$ films can be prepared by numerous deposition techniques, namely, ferrite plating [6, 7], oxidation of metallic films [8], arc plasma method [9, 10], chemical

[4] Author to whom any correspondence should be addressed.
[5] Present address: Eco-Nano-Research Centre, Korean Institute of Science and Technology, POB 131, Cherorayany, Seoul, South Korea.

transport [11, 12], chemical vapour deposition [13–16], sputtering [17], the dip coating process [18], spray pyrolysis [19] and pulsed laser deposition [20]. The main difficulty of these methods is that the substrate during and/or after deposition must be kept at a higher temperature, which imposes restrictions on the selection of the substrate material. A lower temperature method offers many potentially attractive features for material synthesis, particularly when the material is to be used as a simulated corrosion product or a heterogeneous catalyst or as a sensing material.

Very recently, we reported on a novel electrochemical process to prepare nanocrystalline ferrite thin films from aqueous and non-aqueous media at room temperature [21]. This process is a combination of two electrochemical deposition methods, namely, electrodeposition of an alloy (MFe_2, where M is a divalent metal ion) followed by electrochemical oxidation (anodization) of the aforementioned alloy.

One of the less expensive and more popular methods for the preparation of alloy films is electrodeposition [22]. The electrodeposition method has considerable advantages over the other methods of producing alloys because it is relatively easy, technically simple, fast and reproductive and for certain systems it is the only method of preparation [23]. In principle, electrodeposition is possible from both aqueous and non-aqueous solutions. Although deposition in aqueous solutions has practical advantages with respect to industrial manufacture, it is generally unsuitable because reduction of water is kinetically more favourable on most of electrode materials.

We report here the electrodeposition of $NiFe_2$ alloy films from a non-aqueous ethylene glycol sulfate bath on various conducting substrates. The effects of various preparative parameters were studied and optimized to obtain good quality (adherent and uniform) $NiFe_2$ alloy films with very high obtainable thickness. Furthermore these alloy films were electrochemically oxidized in a 1M KOH aqueous electrolyte to convert them to $NiFe_2O_4$ at room temperature. The effects of air annealing of as-prepared $NiFe_2O_4$ thin films were studied on various properties. The films were characterized by using different techniques for their various physical properties.

2. Experimental details

Analar reagent grade (impurities of the order of 10^{-3}%) chemicals (metal sulfates, potassium hydroxide and ethylene glycol) supplied by Loba Chemie, India were used for the bath preparation. The requisite amount of metal sulfate was weighed accurately and dissolved in ethylene glycol to get the desired solution concentration. All the solutions were prepared immediately prior to each deposition. The deposition baths were kept unstirred at a constant, desired temperature. Thin plates (thickness $\sim$ 2–3 mm) of stainless steel, copper and titanium and spray deposited fluorine doped tin oxide (FTO) coated glass (sheet resistance $\sim$ 10–20 Ω cm^{-2}) were used as substrates. The backside of the metal substrates was covered with insulating tape. The cathode deposition area was between 1 and 10 cm^2. The metal substrates were mirror polished with zero grade polish paper, cleaned with detergent, ultrasonically cleaned with double distilled water, rinsed with acetone and methanol and dried. The FTO coated glass substrates were cleaned with 50% dilute HCl followed by detergent, ultrasonically cleaned with double distilled water, then rinsed with acetone and methanol and dried. Just before the deposition, each substrate was anodically etched at a constant current density 2 mA cm^{-2} for 1 min in a bath similar to that used for the deposition.

Polarization measurements were performed to determine the electrochemical deposition potentials of metals and alloys on different substrate materials by using a standard three-

Table 1. Optimized preparative parameters for the deposition of $NiFe_2O_4$ films on various substrates.

I Electrodeposition	
(a) Bath composition	(8 cm^3) 0.1 M $NiSO_4$ + (12 cm^3) 0.1 M $FeSO_4$ (ethylene glycol)
(b) Current density	1.8 mA cm^{-2}
(c) Deposition time	30 min
(d) Bath temperature	27 °C
II Anodization	
(a) Electrolyte	1M KOH
(b) Current density	12 mA cm^{-2}
(c) Intercalation time	20 min
(d) Electrolyte temperature	27 °C

electrode type cell. The reference electrode was a saturated calomel electrode (SCE) and the counter-electrode was a high quality graphite plate.

Galvanostatic deposition of the alloy was performed by applying a constant current density for a certain time. The cathode (substrate) and anode (graphite plate) were mounted parallel to each other at a distance of 5 mm apart.

The bath composition was adjusted to obtain $NiFe_2$ alloy films. Polarization curves were plotted to determine the electrochemical deposition potentials of Ni and Fe metals and the $NiFe_2$ alloy. The effect of current density on deposition current density was studied. The influence of various preparative parameters, including current density, deposition time and bath temperature, on the thickness of the alloy films has been studied. Table 1 shows the optimized preparative parameters for the deposition of good quality $NiFe_2$ alloy on different substrates. The quality of the films was determined by observing uniformity (optical microscopy) and adhesion (tape test) of the films.

To determine the composition of the alloy the deposit was stripped in 20% HNO_3 and analysed for metal content using atomic absorption spectrometry. The cathode current efficiencies were calculated in a conventional manner [24].

The film thickness was determined by using the weight difference method, assuming the bulk density of the $NiFe_2$ alloy (8.20 g cm^{-3}) [24] and $NiFe_2O_4$ (5.37 g cm^{-3}) [25].

The anodization parameters were optimized such that the films would remain adherent to the substrate after anodization. The optimized anodization parameters are given in table 1. The increase in either anodization current density or the optimized time (table 1) resulted in the films peeling off the substrates. Some of the $NiFe_2O_4$ films as-prepared with the above-mentioned conditions (hereafter called NIN1) were annealed in air at different temperatures for different time periods. We found that the films (hereafter called NIN2) annealed at 500 °C for 5 h have better crystallinity than the others.

The structural characterizations of NIN1 and NIN2 films deposited on various substrates were carried out using the x-ray diffraction technique. The x-ray diffraction data of the films were obtained on a Philips PW 3710 x-ray diffractometer using Cu Kα radiation operated at 25 kV and 20 mA. The patterns were taken with zero background intensity using the software facility available with the diffractometer. The grain size of the deposits was the average of the grain sizes estimated from the full width at half maximum (FWHM) of the observed diffraction lines using Scherrer's equation.

The infrared spectrum of the film powder was recorded using a Perkin Elmer infrared spectrophotometer model 783 in the spectral range 200–800 cm^{-1}. The pellet was prepared by mixing KBr with the film powder collected by scratching from the substrate in the ratio

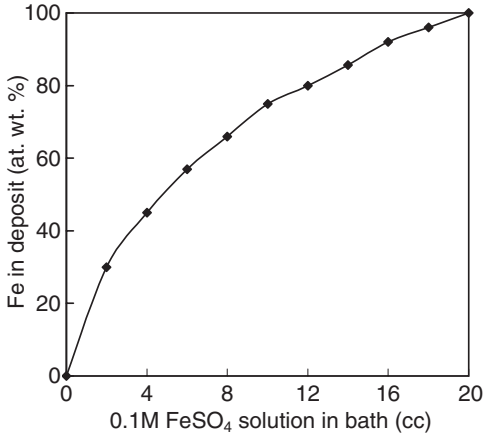

Figure 1. Variation of the amount of Fe in the Ni–Fe alloy deposited with 1.2 mA cm^{-2} current density at room temperature (27 °C) on a stainless steel substrate with a volume of 0.1 M $FeSO_4$ solution in the bath.

300:1 and then pressing the powder between two pieces of polished stainless steel. The noise in the range 200–300 cm^{-1} was due to CO_2 and moisture in the air and hence was not considered.

The surface morphology of the films was studied using atomic force microscopy (AFM) techniques. AFM imaging was carried out with a nanoscope-E (digital instrument) operated in the contact mode. Imaging of the films was performed using silicon nitride probes. The quality of the tip was normally checked by imaging a standard gold ruling for micron resolution and a mica flat surface for atomic resolution.

A Philips CM12 apparatus operated at 120 kV was used for transmission electron microscopy (TEM). A sample for electron microscopy was prepared by putting a film on a copper–carbon grid by dissolving the glass substrate in HF. The dried grid was transferred into a nitrogen-filled container and then to the cell compartment of the TEM microscope, equipped with a Phillips EDAX 9800 analyser. Quantitative EDAX analysis (element detection and analysis by x-ray) of individual particles was carried out with the electron microscope in nanoprobe mode (beam spot size reducible down to 1 nm) using a spot size equal to the average diameter of the particles.

3. Results and discussion

3.1. Film deposition

Composition. Figure 1 shows the typical variation of atomic weight percentage of Fe in the Ni–Fe alloy deposited on a stainless steel substrate at 1.8 mA cm^{-2} current density for 30 min at room temperature (27 °C) with a volume of 0.1 M $FeSO_4$ solution in the bath. It is found that the Ni–Fe alloy deposited from the electrolyte, consisting of (8 cm^3) 0.1 M $NiSO_4$ + (12 cm^3) 0.1 M $FeSO_4$ solution, is $NiFe_2$ and hence it is used for the deposition in the present study.

Electrochemical deposition potential. Figure 2 shows the polarization curves for the reduction of the $NiFe_2$ alloy (A) on different substrates and (B) for different bath temperatures on stainless steel substrates. In all cases, hydrogen evolution during the deposition was observed above the estimated deposition potential, resulting in a less adherent powdery film

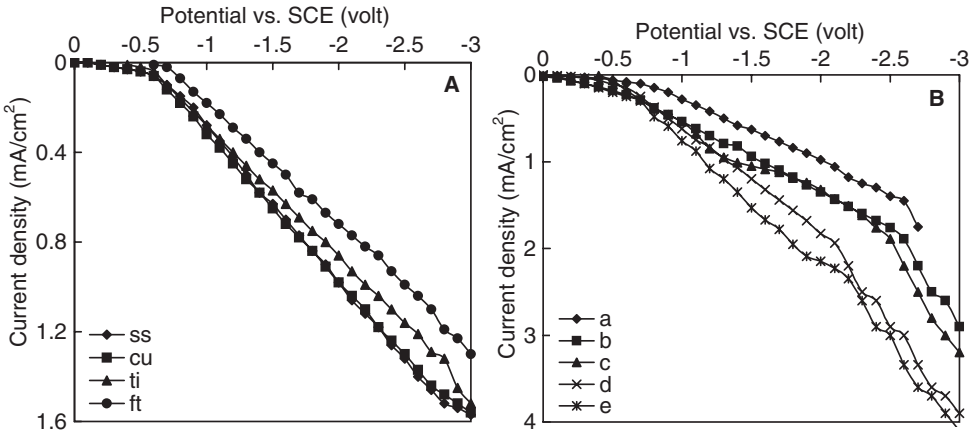

Figure 2. Cathodic polarization curves for the reduction of $NiFe_2$ alloy from non-aqueous bath (A) on different substrates (ss → stainless steel, cu → copper, ti → titanium and ft → FTO coated glass) and (B) for different bath temperatures (a → 27, b → 60, c → 90, d → 120 and e → 150 °C) on stainless steel substrates.

Table 2. Determined electrochemical deposition potentials of Ni and Fe metals and $NiFe_2$ alloy from their respective non-aqueous baths on different substrates at different bath temperatures.

			Deposition potential versus SCE (V)			
Sr. no.	Bath composition	Bath temperature (°C)	Stainless steel	Copper	Titanium	FTO coated glass
1	0.1 M $NiSO_4$	27	−0.78	−0.79	−0.84	−0.86
2	0.1 M $FeSO_4$	27	−0.96	−1.00	−1.12	−1.15
3	(8 cm^3) 0.1 M $NiSO_4$ + (12 cm^3) 0.1 M $FeSO_4$	27	−0.86	−0.89	−1.01	−1.02
4	(8 cm^3) 0.1 M $NiSO_4$ + (12 cm^3) 0.1 M $FeSO_4$	60	−0.85	−0.87	−0.99	−0.98
5	(8 cm^3) 0.1 M $NiSO_4$ + (12 cm^3) 0.1 M $FeSO_4$	90	−0.82	−0.85	−0.94	−0.96
6	(8 cm^3) 0.1 M $NiSO_4$ + (12 cm^3) 0.1 M $FeSO_4$	120	−0.80	−0.82	−0.90	−0.92
7	(8 cm^3) 0.1 M $NiSO_4$ + (12 cm^3) 0.1 M $FeSO_4$	150	−0.79	−0.80	−0.86	−0.88

formation. The estimated deposition potentials of Ni and Fe metals and the $NiFe_2$ alloy from their respective baths are summarized in table 2. It is observed that the deposition potential of $NiFe_2$ lies in between the deposition potentials of Ni and Fe. Deposition potentials are changed for different substrates. An explanation of this change has been discussed previously [24]. It is also seen that the deposition potential decreases as the electrolyte temperature increases due to an increase in the conductivity of the bath.

Current efficiency. During the electrodeposition of the Ni–Fe alloy, some of the applied potential is consumed by side reactions (e.g. hydrogen evolution). The side reactions reduce the current efficiency and can affect the pH at the cathode surface and, therefore, the kinetics of metal reduction [26]. The current efficiency of the Ni–Fe alloy codeposition was calculated

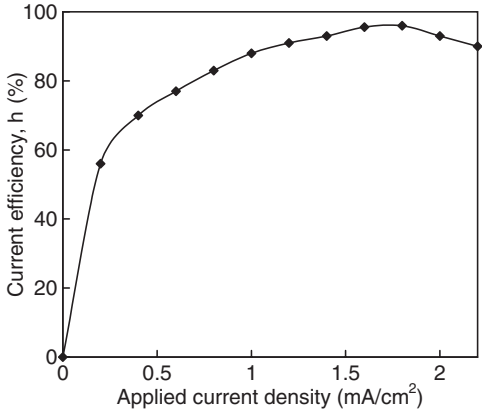

Figure 3. Variation of the current efficiency of the $NiFe_2$ alloy with current density.

by using the simple relation: $100 \times (m_{exp}/m_{th})$, where m_{exp} and m_{th} are experimental and theoretical masses of the Ni–Fe alloy. The deposition of the Ni–Fe alloy was considered as both single metals are reduced in two consecutive steps [27]. The deposited Ni–Fe alloy was stripped and so the atomic absorption spectrometry results are allowed for the nickel and iron weight percentage in the binary alloy. The theoretical mass of Ni–Fe alloy (m_{th}) can be calculated according to Faraday's law. The influence of current density on current efficiency was studied. Figure 3 shows the variation of current efficiency with current density for Ni–Fe alloy deposition onto a stainless steel substrate for 30 min at room temperature. Current efficiency was found to increase initially with increase in current density up to 1.8 mA cm^{-2} and decreased afterwards with further increase in current density. About 96% current efficiency was found at 1.8 mA cm^{-2} current density. Lower current efficiency, below 1.8 mA cm^{-2} current density, is due to a decrease in the rate of deposition of metals to a point where hydrogen evolution is the dominant reaction on the cathode [28]. Further increase in current density above 1.8 mA cm^{-2} only leads to dissociation of ethylene glycol molecules or hydrogen evolution as side reactions, which results in the reduction of current efficiency.

3.2. Film thickness

The effects of current density, deposition time and bath temperature on $NiFe_2$ alloy film thickness were studied. Figure 4 shows the variations of thickness of $NiFe_2$ alloy films deposited on stainless steel substrates with (A) current density, (B) deposition time and (C) bath temperature. It has been observed that the $NiFe_2$ alloy films deposited on different substrates at room temperature with 1.8 mA cm^{-2} current density for 30 min have a thickness of $1.8(\pm 0.2)$ μm. Further increase in current density or deposition time resulted in a decrease in the film thickness, possibly due to porous, foggy and less adherent film formation. Also the films may have tensile stress, which tends to cause delamination, resulting in the films peeling off the substrates when they became thick [29, 30]. The reduction in film thickness with increase in bath temperature above room temperature may be due to a higher rate of dissolution than deposition of the films.

The NIN1 thin films have almost the same thickness as that of the alloy. The change in thickness after annealing is also not considerable.

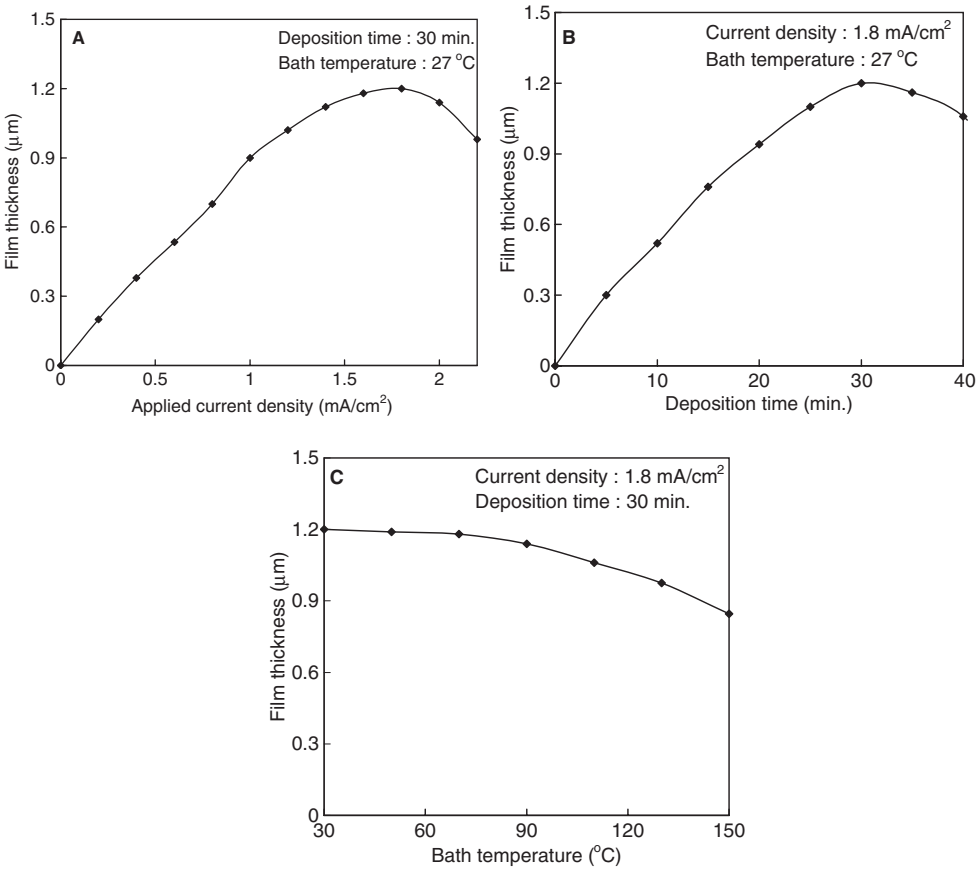

Figure 4. Variation of $NiFe_2$ alloy film thickness with (A) current density, (B) deposition time and (C) bath temperature deposited on stainless steel substrate.

3.3. Crystal structure

The x-ray diffraction patterns of the (A) NIN1 and (B) NIN2 thin films deposited on various substrates were studied to analyse texture and grain size. Typical x-ray diffractograms of (A) NIN1 and (B) NIN2 thin films deposited on stainless steel substrates are shown in figure 5. The agreement of the observed '*d*' values for the peaks in the diffractograms with standard [25] JCPDS '*d*' values (table 3) reveals that the films possess the single-phase spinel cubic $NiFe_2O_4$ crystalline structure. All the films are polycrystalline in nature. Moreover, the unaccounted reflections due to unwanted crystallites such as Ni–O, Fe–O, etc are absent in the films. Since the deposition conditions were identical for the films deposited on all the substrates, differences in texture must be attributed to the different substrate crystallite orientations (observed from XRD studies not shown here) for different substrates. After annealing, a sharper and more intense diffraction peak due to the (311) plane (expected for spinel structure [25]) is observed for the films deposited on various substrates. This observation suggests that the nucleation of a spinel phase takes place after anodization and the crystallization process is completed after annealing.

The calculated values of lattice constant '*a*' of the films on various substrates are listed in table 3. The value of the lattice constant increased after annealing, indicating that the increase

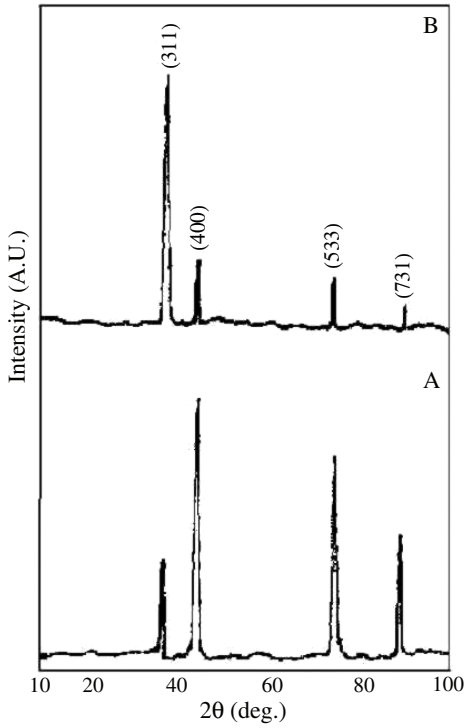

Figure 5. Representative x-ray diffraction patterns of (A) NIN1 and (B) NIN2 films deposited on stainless steel substrates.

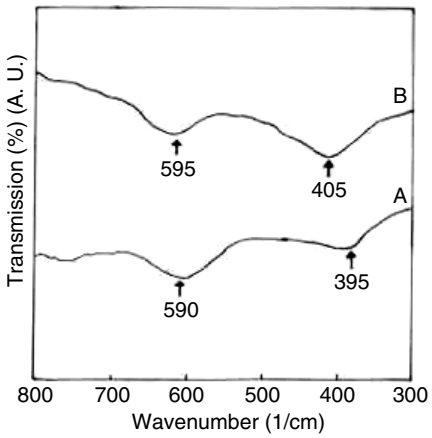

Figure 6. IR spectra of NIN1 and NIN2 film powders.

in strain in the films may be due to a mismatch between either the lattice constant or the thermal expansion coefficients of the film and the substrate materials after annealing.

The calculated average grain sizes are listed in table 3. The average grain sizes of the films on various substrates are below 40 nm, predicting the nanocrystalline nature of the films. The increase in grain size after annealing is not significant.

The room temperature IR spectra of NIN1 and NIN2 film powders are shown in figure 6.

Table 3. X-ray diffraction studies of (A) NIN1 and (B) NIN2 films deposited on various substrates.

	Standard		Observed				Plane	Lattice constant 'a' (Å)		Average grain size (nm)	
			'd' (Å)		I/I_0 (%)						
Substrate	'd' (Å)	I/I_0 (%)	A	B	A	B	(hkl)	A	B	A	B
Stainless steel	2.51	100	2.50	2.51	39	100	311				
	2.08	22	2.08	2.08	100	22	400	8.33	8.34	16	26
	1.27	2	1.27	1.27	83	18	533				
	1.09	3	1.09	1.09	50	8	731				
Copper	2.51	100	2.50	2.51	57	100	311				
	2.08	22	2.08	—	100	27	400	8.33	8.34	21	31
	1.27	2	1.27	1.27	45	47	533				
	1.09	3	1.09	1.09	67	33	731				
Titanium	2.51	100	2.50	2.51	47	100	311				
	1.47	34	1.47	1.48	78	26	440				
	1.32	2	1.34	1.34	100	60	620	8.34	8.35	16	25
	1.25	1	1.25	1.25	29	13	622				
	1.11	1	—	1.12	—	6	642				
FTO coated glass	2.51	100	2.51	2.51	58	100	311				
	1.70	9	1.68	1.68	27	12	422	8.34	8.35	17	28
	1.47	34	1.47	1.48	43	33	440				
	1.08	3	1.08	1.08	100	17	731				

The spectra show a high frequency band (ν_1) around 600 cm^{-1} and a low frequency band (ν_2) around 400 cm^{-1} as a common feature of a spinel ferrite. The bands at 400 cm^{-1} and around 600 cm^{-1} are assigned to the intrinsic vibration of tetrahedral and octahedral complexes [31]. It is observed that the positions of high frequency (ν_1) and low frequency (ν_2) bands are located at $\nu_1 = 590$ and 595 cm^{-1} and $\nu_2 = 395$ and 405 cm^{-1} for powders of NIN1 and NIN2 films, respectively. This difference in the band positions is observed because of a difference in the Fe^{3+}–O_2 distance for tetrahedral and octahedral complexes, possibly due to the difference in the grain size and processing temperature.

3.4. Surface morphology microstructure and composition

Typical topographical views (AFM images) of (A) $NiFe_2$ alloy, (B) NIN1 and (C) NIN2 films deposited on FTO coated glass substrates are displayed in figure 7. All the films are indicated to consist of granular nanosized grains. Due to the intercalation of oxygen species during anodization, island-like structures are observed for NIN1 film. However, a slight increase in grain size with homogeneous, uniform and compact surface morphology is observed after annealing. This probably suggests that the nucleation of the spinel phase takes place inside the amorphous-like grains in the NIN1 film and the crystallization process is completed after annealing as evidenced from XRD studies. This consideration may be reasonable in view of energy conservation because the nucleation occurring inside the grains can only be completed through the rearrangement and short-distance diffusion of oxygen atoms. Thus the crystallization process is not accompanied by obvious grain growth.

A typical low magnification TEM micrograph of NIN2 film deposited on an FTO coated glass substrate shows agglomeration of very fine particles (figure 8), which is a feature usually observed when chemical synthesis is used [32]. Inset (B) in figure 8 shows a high-resolution

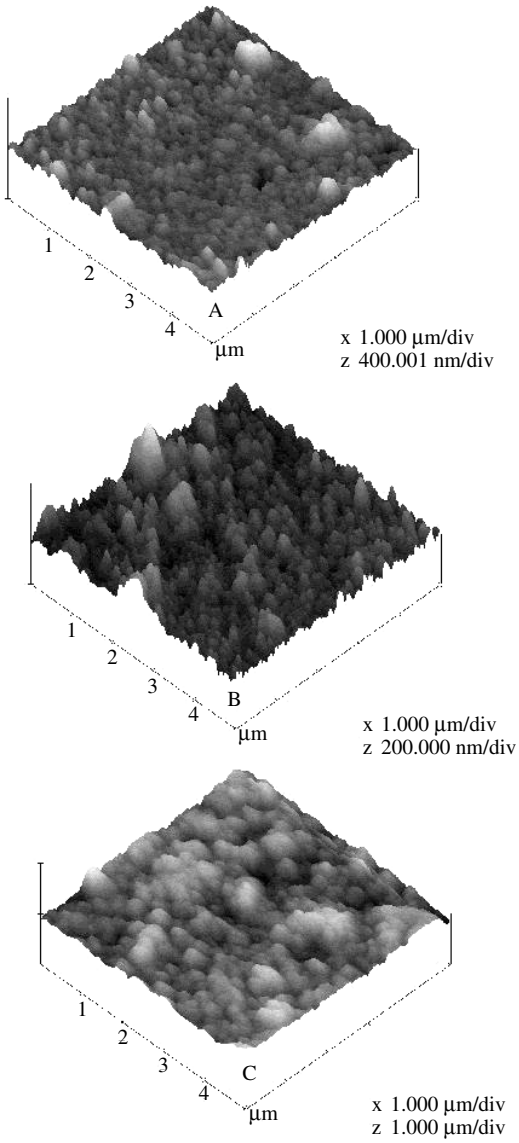

Figure 7. Typical AFM images of (A) $NiFe_2$ alloy, (B) NIN1 and (C) NIN2 films deposited on FTO coated glass substrates.

micrograph (HRTEM), and indicates that the film is composed of crystal grains with diameters of about 10 nm. The difference in grain sizes obtained by XRD and HRTEM techniques is due to the basic difference between the techniques. XRD gives a much better average over a large, bulk volume while TEM is limited to a few grains which are electron transparent, therefore, TEM always results in a smaller grain size than XRD. By HRTEM, it is also possible to detect the typical lattice plane for cubic structured $NiFe_2O_4$ particles. Inset (C) in figure 8 shows the result obtained after Fourier transformation of the micrograph. The $NiFe_2O_4$ particles crystallize into a cubic close packed lattice with an average inter-particle separation (core to core) of 0.33 nm. The lattice plane of the HRTEM lattice image is (220) of the cubic crystal structure.

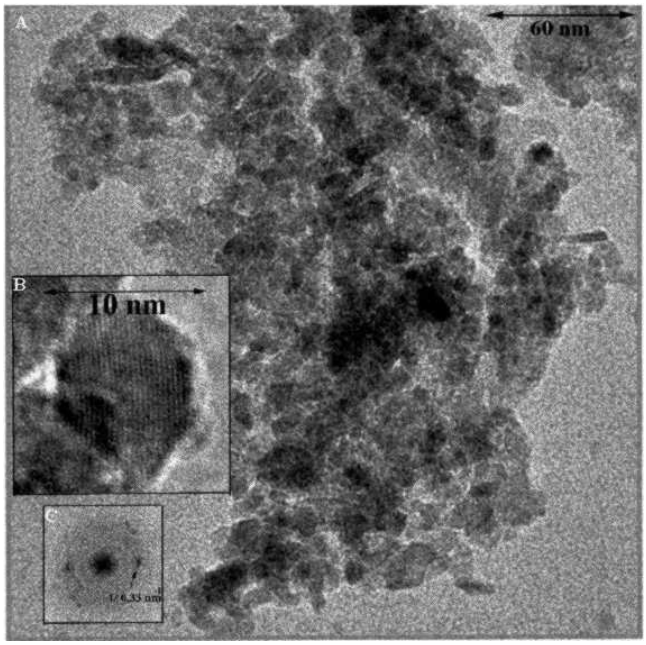

Figure 8. (A) Typical low magnification transmission electron micrograph of a NIN2 film deposited on an FTO coated glass substrate. Inset (B) shows a high-resolution micrograph (HRTEM). Inset (C) shows the result obtained after Fourier transformation of the micrograph.

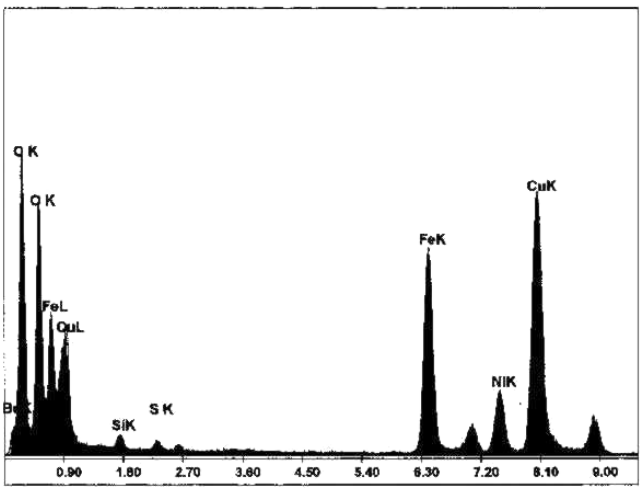

Figure 9. Typical EDAX pattern of the NIN2 film on an FTO coated glass substrate.

The quantitative elemental composition of the films was determined by using an EDAX analyser attached to the transmission electron microscope. Figure 9 shows a typical EDAX pattern of the NIN2 film deposited on the FTO coated glass substrate. The observed impurity peaks of Be and S are due to the substrate, which has been previously verified. This method is quite uncertain for the quantitative analysis of light elements like oxygen. Our EDAX study reveals a percentage of Fe in the film in excess of that required to give an Ni:Fe atomic weight percentage ratio of 1:3.

4. Conclusions

Room temperature deposition of nanocrystalline $NiFe_2O_4$ thin films with thickness 1.8 ($\pm$0.2) μm on different conducting substrates is possible by electrodeposition of $NiFe_2$ alloy from a non-aqueous ethylene glycol sulfate bath followed by electrochemical oxidation (anodization) of the alloy in an aqueous bath. Electrodeposition of $NiFe_2$ alloy films on different substrates with 96% current efficiency is possible from an ethylene glycol sulfate bath. The $NiFe_2O_4$ films have spinel cubic structures with average grain size between 10 and 40 nm. The films cover the substrates well with a homogeneous and uniform surface. The nucleation of the spinel phase takes place after anodization and air annealing at 500 °C for 5 h is necessary for completion of the crystallization process. After annealing, the crystallinity and morphology of the films improve with a slight increase in grain size.

Acknowledgment

One of the authors (SDS) acknowledges the Department of Physics, Shivaji University, Kolhapur, India for providing the necessary facilities and the Alexander von Humboldt Foundation, Germany for financial support.

References

[1] Ishino K and Naramiya Y 1987 *Am. Ceram. Soc. Bull.* **66** 1469
[2] Zhang Q, Itoh T, Abe M and Tamaura Y 1992 *Ferrites Proc. ICF-6 (Tokyo, 1992)* ed T Yamaguchi and M Abe p 481
[3] Dube G R and Darshane V S 1993 *J. Mol. Catal.* **79** 285
[4] Gopal Reddy C V, Manorama S V and Rao V J 1999 *Sensors Actuators* B **55** 90
[5] Satyanarayana L, Madhusudan Reddy K and Manoram S V 2003 *Mater. Chem. Phys.* **82** 21
[6] Abe M, Itoh T, Tamaura Y and Gomi M 1998 *J. Appl. Phys.* **63** 3774
[7] Itoh T, Abe M, Sasao T and Tamaura Y 1989 *IEEE Trans. Magn.* **25** 4230
[8] Suran G and Heurtel A 1972 *J. Appl. Phys.* **43** 536
[9] Dillon J F 1970 *J. Appl. Phys.* **41** 1348
[10] Naoe M and Yamanaka S 1970 *Japan. J. Appl. Phys.* **9** 293
[11] Marshall D J 1971 *J. Cryst. Growth* **9** 305
[12] Gibart P, Robbins M and Kane A B 1974 *J. Cryst. Growth* **2425** 166
[13] Pulliam G R 1967 *J. Appl. Phys.* **38** 1120
[14] Mee J E, Pulliam G R, Archer J L and Besser P J 1969 *IEEE Trans. Magn.* **5** 717
[15] Fitzgerald A G and Engin R 1974 *Thin Solid Films* **20** 317
[16] Itoh H, Takeda T and Naka S 1986 *J. Mater. Sci.* **21** 3677
[17] Venzke S, Van Dover R B, Phillips J M, Gyorgy E M, Siegrist T, Chen C H, Werder D, Fleming R M, Felder R J, Coleman E and Opila R 1996 *J. Mater. Res.* **11** 1187
[18] Tsuchiya T, Yamashiro H, Sei T and Inamura T 1992 *J. Mater. Sci.* **27** 3645
[19] Deschanres J L, Langlet M and Joubert J C 1990 *J. Magn. Magn. Mater.* **83** 437
[20] Kiyomura T and Gomi M 1998 *J. Magn. Soc. Japan* **22** 179
[21] Sartale S D, Bagde G D, Lokhande C D and Giersig M 2001 *Appl. Surf. Sci.* **182** 366–71
[22] Brenner A 1963 *Electrodeposition of Alloys* vol 1 and 2 (New York: Academic)
[23] Matlosz M 1993 *J. Electrochem. Soc.* **140** 2272
[24] Sartale S D and Lokhande C D 2000 *Indian J. Eng. Mater. Sci.* **7** 404
[25] JCPDS-ICDD card no. 44-1485 1994
[26] Zech N and Lincot D 2000 *Electrochem. Acta* **45** 3461
[27] Sartale S D, Lokhande C D and Müller M 2003 *Mater. Chem. Phys.* **80** 120
[28] Sasaki K and Talbot J B 1998 *J. Electrochem. Soc.* **145** 81
[29] Thornton J A 1986 *J. Vac. Sci. Technol.* A **4** 3059
[30] Kitamoto Y and Abe M 1997 *J. Physique Coll.* IV **7** C1 595
[31] Labde B K, Sable M C and Shamkuwar N R 2003 *Mater. Lett.* **57** 1651
[32] Hishinuma K and Akiba T 1995 *Bull. Mater. Sci.* **18** 811